Cement and Concrete Composites 88 (2018) 172–186

Contents lists available at ScienceDirect

Cement and Concrete Composites

journal homepage: www.elsevier.com/locate/cemconcomp

Nacre-inspired composite design approaches for large-scale cementitious members and structures

Daniel G. Soltan [a], Victor C. Li [a, b, c, *]

[a] Macromolecular Science and Engineering, University of Michigan, 2800 Plymouth Road, Rm. 3006E Building 28 NCRC, Ann Arbor, MI, 48109, USA
[b] Civil and Environmental Engineering, University of Michigan, 2350 Hayward Ave., Ann Arbor, MI, 48109, USA
[c] Materials Science and Engineering, University of Michigan, 2300 Hayward Ave., Ann Arbor, MI, 48109, USA

ARTICLE INFO

Article history:
Received 11 September 2017
Received in revised form
17 November 2017
Accepted 9 February 2018
Available online 15 February 2018

Keywords:
Bio-inspired
Cementitious composites
Energy dissipation
Mesh reinforcement
Fiber reinforced
Strain-hardening cementitious composites

ABSTRACT

Nacre boasts a remarkable mechanical property profile, despite being composed 95% of a chalk-like mineral. Previous research has reported the features and deformation mechanisms responsible, inspiring many synthetic, biomimetic versions of nacre. However, due to processing challenges associated with nacre's complex structure, this composite design inspiration has not been applied on a scale useful for civil engineering applications. This research investigates the utility of nacre's composite design on a scale relevant to infrastructure by exploiting the "distributed microcracking" behavior of strain-hardening cementitious composites (SHCCs). With the goal of emulating nacre's deformation mechanisms, rather than simply structural mimicry, various design approaches within the constraints of construction practices are introduced and evaluated in direct tension and beam bending. An alternating layering scheme, using a geotextile mesh and a high strength SHCC, is seen to produce promising behavior, significantly outperforming the high strength SHCC in its monolithic form. Advantages are seen in tension, compression, and particularly flexure. The deformation mechanisms responsible for this enhanced performance, and those of alternate approaches, are discussed.

1. Introduction

1.1. Bio-inspiration from nacre

Nacre, the iridescent material seen on the interior of shells like that of the abalone, is one of the seminal natural materials to motivate the biomimicry/bio-inspiration paradigm across science and engineering disciplines. Previous research has illuminated how nacre is able to exhibit an impressive combination of high compressive strength, high tensile strength, and high tensile ductility, despite being composed 95% of a relatively weak and brittle, chalk-like mineral called aragonite [1–9]. Nacre has been shown to require 1000–3000 times as much energy to cause failure than the bulk form of its principal component, aragonite [3,8]. Nacre is a shining example of nature's ability to leverage structure via shaping to turn a relatively limited palette of compositional building blocks (Oxygen, Hydrogen, Carbon, Nitrogen, Calcium, Magnesium etc.) into an immense and diverse ecosystem of materials, many of which outperform deliberately human-engineered materials in a variety of ways [7,10,11].

It has been seen that the structuring of nacre promotes specific deformation mechanisms that are responsible for the dramatic transformation of brittle aragonite into a material that exhibits tremendous toughness (the amount of energy required to cause the material to fail) [1,2,4–9]. There are four principle features of nacre's hierarchical structuring that have been observed and reported to be key in these deformation mechanisms. Nacre is composed of (1) distinct layers, with primary mineral layers composed of (2) discrete, tiled, hexagonal aragonite tablets, with boundaries off-set from those of the tablets in the layers above and below, each tablet having a (3) markedly rough or wavy surface that nests into adjacent mineral layers, as well as (4) secondary, thin bio-polymeric layers between mineral tablets, which allow sliding of the tablets relative to each other, while also providing some physical resistance as sliding progresses [1]. This structure has been visually

Abbreviations: SHCCs, Strain-hardening cementitious composites, also called Engineered Cementitious Composites (ECCs), or "bendable concrete"; PP, Polypropylene; VCP, Vinyl-coated polyester; %CM, percentage of total cementitious material, by weight.

* Corresponding author. Civil and Environmental Engineering, University of Michigan, 2350 Hayward Ave., Ann Arbor, MI, 48109, USA.
E-mail addresses: dsoltan@umich.edu (D.G. Soltan), vcli@umich.edu (V.C. Li).

https://doi.org/10.1016/j.cemconcomp.2018.02.006
0958-9465/

documented previously by Barthelat et al. (2007) [1], among others, and has often been referred to as a "brick-and-mortar" arrangement. However, in literal brick and mortar structures, the mortar does not allow for the stretching or "give" within a given layer, nor the shear sliding between layers—both of which are key for the deformation mechanisms observed in nacre.

The deformation mechanisms seen in nacre allow a combination of tensile strength and ductility, macroscale tensile strain-hardening and shear-hardening behavior, and flaw and damage tolerance, each of which contribute to material toughness. The discrete tablets allow a "give" in the structure under tension and shear, which, as a result of local slip-hardening mechanisms, can be distributed throughout the material, instead of localizing at weak points and stress concentrations. These deformation mechanisms suppress brittle failure, increasing durability, and controlling damage such that it can later be repaired through natural processes, promoting resilience in the material.

Nacre's impressive mechanical performance has inspired a multitude of synthetic nacre materials [12–16]. However, these previous attempts at mimicry of nacre's structure have shared the same thin-sheet size scale and/or slow manufacturing/growth processes of natural nacre, making them irrelevant for large-scale structural applications. A major bottle neck in the development of synthetic, nacre-inspired materials is the time and cost-efficient arrangement of myriad tablet elements, which is particularly challenging for feasible, scalable manufacturing at large size scales.

1.2. Improved structural cementitious materials via inspiration from nacre

Concrete, by both weight and volume, is the most widely used engineering material in the world. It can be processed in large quantities, is relatively cheap, and performs efficiently in compression, and therefore serves as the ubiquitous basis of our built environment.

However, concrete is not without severe limitations. Weak and brittle in tension, concrete fails under many typical loading modes and environmental conditions—catastrophically in extreme cases. A single crack can lead to rapid deterioration or cause total loss of load carrying capacity. As such a proliferate component of civil infrastructure, concrete's shortcomings are evident in our everyday life, from poor road conditions and deteriorating bridges, to the frequent and disruptive repairs of this infrastructure, despite the use of steel reinforcements. The failures due to concrete's lack of durability and resiliency are not just an inconvenience to the public and drain on governmental budgets, but also threats to human safety and the well-being of our modern societies.

These shortcomings make concrete infrastructure unsustainable. Concrete's lack of durability and resiliency demand repeated repair events that consume valuable resources, like time, energy, and money. In the US, the deterioration caused by these issues is occurring at a rate greater than at which it can be repaired, evidenced by the "D+" grade of the nation's infrastructure condition as assigned by the American Society of Civil Engineers in their latest annual report card [17]. Additionally, the repair events that can be completed are responsible for the majority of the carbon emissions (a measure of environmental impact) of concrete infrastructure, mainly due to traffic disruption [18]. Truly sustainable infrastructure would instead have long service life, dramatically reduced environmental impact, and the capacity to endure loading conditions, both of the present and of the future.

Beyond durability under normal service conditions, concrete infrastructure also needs to withstand extreme loading events to ensure human safety in events like naturally occurring disasters, and even malicious attacks, of seemingly unlikely scale. Resiliency, defined as the ability to minimize the probability of failure, minimize the consequences of failure, and minimize the time between failure and a return to service, is also a shortcoming of typical concrete. An improvement of the durability and resiliency of the concrete material used in critical infrastructure components would effectively address each of the requirements for sustainable infrastructure, significantly improving the sustainability of our built environment and the functioning of our modern societies.

To address the shortcomings in durability and resiliency of concrete, we look to nature, which seems to have already solved this problem. Can the composite design strategies observed in nacre to boost tensile strength and material toughness in an otherwise weak and brittle material be effective on a much larger scale, such as that which is applicable to civil infrastructure? This study aims to answer that question and explore ways this can be achieved.

As previously noted, nacre's impressive mechanical performance is due to its structuring and deformation mechanisms associated with that structuring. This improvement in performance has been determined to be derived from the aforementioned shaping paradigm of natural materials. A portion of this improvement is likely a product of size effects associated with the micron sized aragonite tablets (~8 μm in diameter, 0.5 μm thickness), as discussed by Rim et al. [15]. For realistic, widely applicable structural building materials, it is not feasible to exploit size effects due to processing constraints associated with the scale of the end-product. This research focuses, instead, on the contributions of shaping considerations, other than size effects, to the improvement of mechanical performance of nacre over that of bulk aragonite, and how those shaping strategies can be adapted for application in large-scale, structural building materials.

1.3. Large-scale nacre-inspired structure via ECCs

Engineered cementitious composites, also known as ECCs or "bendable concrete", are strain-hardening cementitious composites (SHCCs) incorporating a low volume fraction of short polymer fibers and exhibit a characteristic distributed microcracking pattern when subjected to tensile loading above the elastic limit. The micromechanics of ECCs have been described previously in detail [19], and differ from those of other fiber reinforced concretes. In short, when the brittle cementitious matrix first fractures in tension, the dispersed fibers are able to bridge the crack, holding the crack to several tens of microns in width, while carrying the tensile load such that further opening of the microcrack (via fiber pullout) requires more energy than originating a microcrack elsewhere in the matrix. This cycle can be repeated many times, such that the composite is able to distribute deformation throughout and suppress brittle fracture failure.

The characteristic distributed microcracking tensile behavior of ECC provides a convenient route to produce an approximated analog of the natural nacre structure. When strained in tension, a plurality of microcracks open in the ECC material at the weakest locations in the cementitious matrix, leaving between them stronger, discrete units, analogous to the tablets in nacre. Under unidirectional tension, the analog discrete units would be strips, rather than tablets, however, microcracks will occur in an orientation normal (perpendicular) to any tensile loading direction, so if tensile stress is applied in multiple directions, tablet-like architecture would theoretically be generated. Moreover, ECC produces a "give" at a certain threshold tensile stress, while also providing resistance to continuing tensile strain (as evidenced by the tensile strain-hardening behavior), just as in nacre.

When layers of ECC are stacked, an approximation of the nacre structure can be created. Microcracks opening in each of the ECC

layers are probabilistically unlikely to line up, producing the off-set arrangement of stacked discrete units like that of nacre. In this way, crack propagation could be manipulated to require a higher amount of energy to cause failure.

Similar to nacre's ability to control damage to a degree that it can later be repaired via natural processes, ECC's microcracks are held to tight widths (tens of microns across) that allow cracks to self-heal with exposure to water and air [20]. This previously documented behavior of ECCs can be leveraged in a nacre-inspired composite scheme to lend resilience.

Using ECCs to approximate the nacre structure in a form applicable to civil infrastructure is appealing because it provides an efficient solution to the principal challenge of producing synthetic nacre-inspired materials: the arrangement of the myriad discrete units.

While ECCs themselves are inherently a more durable, resilient alternative to typical, brittle concrete materials [19,21], this study seeks to determine if material design lessons learned from nacre can *further* improve the performance of ECCs, in addition to determining if these lessons are applicable and have utility on size scales relevant for civil infrastructure.

Preliminary testing [22] showed that nacre-inspired layering and waviness, applied to an ECC material, enhanced composite performance in flexure, boosting inelastic flexural toughness by as much as 140%. The work presented here investigates the performance of additional nacre-inspired design schemes in flexure, as well as in direct tension. The most promising design schemes are characterized in compression.

Rather than devise an optimized large-scale building material or product, this investigation aims to determine how nacre-inspired composite design features and approaches can affect the mechanical performance of structural cementitious materials on a size-scale much larger than that of natural nacre. Lessons learned from this study may be applied to develop cementitious composite materials and members for critical infrastructure components requiring extreme toughness, durability, and resiliency. Structural components designed for seismic, impact, and blast resistance/mitigation are prime candidates for such improvements in mechanical performance.

2. Materials and methods

2.1. Compositional materials

A high strength ECC material, originally developed by Ranade et al. (2011), is used as the basis of all the nacre-inspired composite designs investigated herein [23,24]. The composition of this material, referred to henceforth as HSHDC (high strength, high ductility concrete) is described in Table 1. The compositional ratios in Table 1 are reported as the percentage of the total cementitious material by weight (%CM), where the Type H cement and microsilica (also called silica fume) are considered cementitious material. A 2% volume fraction of ultra high molecular weight polyethylene (UHMW-PE) polymer fibers are included. Additional information about the ingredients of the HSHDC composition can be found in Appendix I and in Ranade et al. (2011) [24]. This composition and its mixing procedure is kept consistent throughout the study.

The mixing process of the HSHDC is highly compatible with typical concrete mixing equipment, however, the highly densified nature of the material requires a particular sequence of ingredient addition to ensure proper mixing and dispersion of fibers. The mixing procedure used for this study is described in Appendix II.

This study does not investigate the HSHDC material per se; rather, it is the nacre-inspired structuring approaches that are investigated. The structuring approaches considered in this study

Table 1
The compositional ratio of the HSHDC material used as the primary component of each bio-inspired composite design investigated in this study. Composition is reported here as percentage of the total cementitious, except fiber content.

Ingredient	%CM
Class H Cement	72.00
Microsilica	28.00
Ground Silica	19.90
F-60 Sand	50.40
Water	[a]15.00
HRWRA	1.30
Coupling Agent	0.75
UHMW-PE Fiber	2.00% by vol.

[a] Plus water content of soaked fibers: 0.3–0.4 g water per gram of total fibers (dry weight).

are designed to be applicable with any strain-hardening cementitious composite that has been designed for casting. The HSDHC material is simply a model ECC/SHCC material that was selected for this study to explore if the hypothesized strength and toughness enhancing benefits of the nacre-inspired could potentially push ECC performance into a materials performance "whitespace" —a previously unachieved property profile.

Several of the nacre-inspired design schemes introduce additional materials into the composite. A commercially available, high strength polyurethane-based adhesive is used for one scheme, and a variation of that scheme. Polymer mesh materials are used for several other schemes. One mesh is a commercially available, polypropylene geotextile mesh ("PP-Mesh") marketed for soil stability and soil separation in large-scale landscaping/construction applications. It is alkali resistant and rated for a 75 year service life, per a manufacturer-provided data sheet. Use of a vinyl-coated polyester mesh ("VCP mesh"), marketed as a tear-resistant window/door screen material, is also investigated. The appearance of these polymer meshes is described and compared in Fig. 1.

2.2. Mechanical testing methods

This study seeks to compare the performance of the structured composite design schemes to that of the monolithic HSHDC

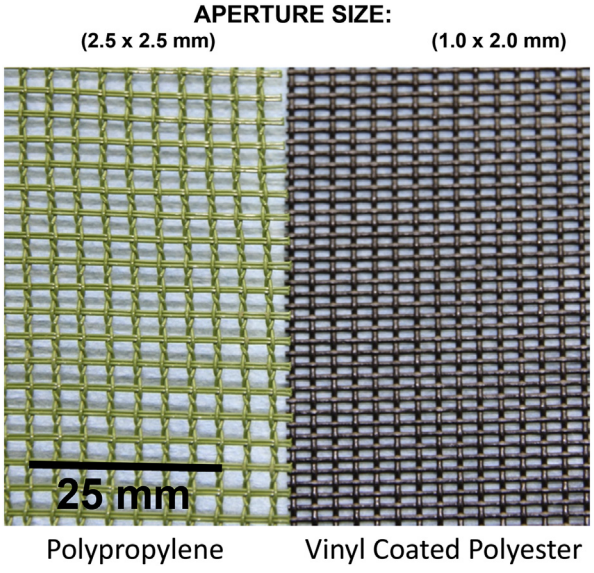

Fig. 1. The appearance of the two polymer meshes used in this study are compared.

material to determine mechanical performance benefits produced by the nacre-inspired design schemes. Performance is compared in direct tension, beam bending (flexure), and compression. Specimens are tested between 14 and 19 days after casting, following an accelerated curing process (see Appendix II).

Testing in direct tension is performed on a 110kip (490 kN) load capacity Instron instrument, using large-scale dogbone shaped specimens to accommodate the various nacre-inspired layering schemes described in Section 3. The size and shape of large dogbone shaped specimen is depicted in Fig. 2. A pre-loading rate of 0.75 mm/min is used to allow the specimens to settle into the grip fixtures. When a pre-load of ~2 kips (8.9 kN) is achieved, the loading rate is increased to 1 mm/min and data collection is started.

Tensile stress is computed based on measurements of the gage section cross-section of each individual specimen. Tensile strength for each bio-inspired scheme is recorded as the average of the maximum stress carried by each specimen. Strain capacity is recorded as the tensile strain value at the maximum stress, based on change in gage section length as measured by LVDTs attached to each specimen.

Four-point bend testing is performed using a 22 kip (97.9 kN) load capacity MTS universal testing machine. A support span of 10 inches (25.4 cm) is used with a loading span of 3.5 inches (8.89 cm). Fixed displacement loading was applied while load and "average third point displacement" were recorded. Average third point displacement is a measurement of displacement at the top two loading support points, as measured by instrument stroke during testing. Beam specimens with approximate height of 75 mm and width of 68 mm are used. Because specimens are sectioned to size, and each have slightly different dimensions, every specimen is measured prior to testing and those measurements are used to calculate the flexural stress for each specimen individually. Flexural stress is calculated according to Equation (1), where F is force in newtons, L is the support span (254 mm), b is the width of the specimen, and d is the height.

$$\text{Flexural Stress, } \sigma_f = (FL)/(bd^2) \quad (1)$$

Modulus of rupture is calculated as the maximum flexural stress carried by a specimen. Inelastic flexural toughness is also calculated, providing a convenient metric to compare the toughness of the composites in flexure. The process of calculating inelastic flexural toughness is described in Soltan et al. (2014) [22], and is a function of the elastic limit in flexure, the modulus of rupture, and the deflection at which the stress carrying capacity of the beam has decayed to 90% of the modulus of rupture, after peak load has been reached.

Compression testing was performed with a Forney compression machine using cube-shaped specimens. A loading rate of ~50 psi/s (~0.345 MPa/s) was used, based on recommendations of the ASTM C109 International standard. Compressive strength is reported as the stress at the maximum load sustained by the composite.

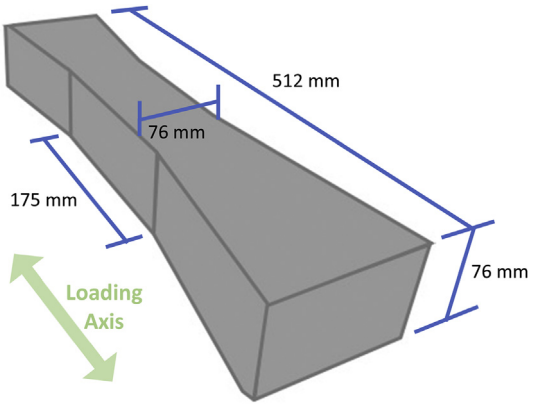

Fig. 2. The large dogbone shaped specimens have a gage section cross-section approximately 76 × 76 mm, and gage length of ~175 mm. Specimens are loaded along the major axis.

3. Approaches to physical modeling of the nacre-inspired structure

The nacre-inspired composite design schemes investigated herein are summarized in Table 2. These physical models are used to determine the potential mechanical utility of nacre-inspired design features in cementitious material systems on a size scale much larger than that of natural nacre. To determine these effects, the nacre-inspired schemes are compared to the monolithic version of the same ECC material (HSHDC) that serves as the primary component of all the nacre-inspired design schemes. The general nacre-inspired design philosophy and approach, and full description of each of the schemes are included in Appendix III.

There are two main approaches to the physical adaptation of nacre's structure and deformation mechanisms to a large-scale structural material reported here. The first, illustrated in Fig. 3, is stacking multiple layers of precast ECC in various ways and manipulating the interface between the layers (type: "Stacked"). The second approach is creating distinct layers within the cementitious composite via inlayed mesh materials (type: "Mesh"), as illustrated in Fig. 4. Each approach incorporates approximations of key features seen in nacre through different processing and compositional routes.

It should be noted that the primary aim of using the mesh materials here is to create distinct layers and other nacre-inspired structural features (e.g. interlayer mineral pillars and interfacial surface roughness (Fig. 5), and wavy, nested shaping of the layers (Fig. 6)) previously proposed to be responsible for nacre's resistance to layer sliding and overall mechanical performance [1,4,5,7,9,25–27]. The nacre-inspired mesh layering approach allows adaptions of all of those features to be incorporated simply in a single hierarchical ECC-based composite feasible for large scale construction.

Previous research has shown advantages to using mesh reinforcement in concrete to enhance performance in flexure [28–30]. Peled and Bentur (2003) tested knitted and woven polymer fabrics within cementitious matrices and reported both improved and reduced performance in flexure, depending on the geometry of the fabric, in comparison to continuous fiber reinforcement [28]. Brückner et al. (2006) reported a strengthening effect in rectangular beams and T-shaped beams when multiple layers of woven glass fabrics were cast into the concrete [29]. Pakravan et al. (2011) saw enhanced ductility via displacement-hardening behavior (in flexure) when non-woven polypropylene fabric was added to a cementitious matrix, though the addition of many fabric layers caused a loss in flexural strength [30].

Effects of textile reinforcement or layering on composite performance in direct tension have not been as thoroughly reported, and are investigated in the present study. This study also investigates the utility of mesh materials for hierarchical structuring performance benefits beyond simple reinforcement. The "PP-mesh WD-40" series is included to determine the reinforcing contribution of the mesh to tensile and flexural performance.

Similarly, the "monolithic layered casting" series is included to determine the preferential fiber alignment contribution to tensile and flexural performance.

Table 2
The nacre inspired composite design schemes and the control schemes are labeled and described. See Appendix III for full descriptions for each scheme.

Type	Label	Description
Summary of composite design schemes		
Monolithic	Pour casting	Typical large application processing, material poured into mold
	Layered casting	Mold filled in step-wise fashion to promote preferential fiber alignment
Stacked	PU-bonded	Pre-cast HSHDC layers (3 and 4 layer versions) with PU adhesive at interfaces
	PU-bonded Prestrained	Same as above with HSHDC strained uniaxially prior to interfacial bonding
	Hybrid	Pre-cast layers alternated with freshly cast layers, no interfacial material
Mesh	PP-mesh	HSHDC alternated with PP-mesh layers (3 and 5 mesh layer versions)
	VCP-mesh	HSHDC alternated with VCP-mesh layers (3 and 5 mesh layer versions)
	PP-mesh WD40	HSHDC alternated with PP-mesh layers (3) coated in mold release (WD40)

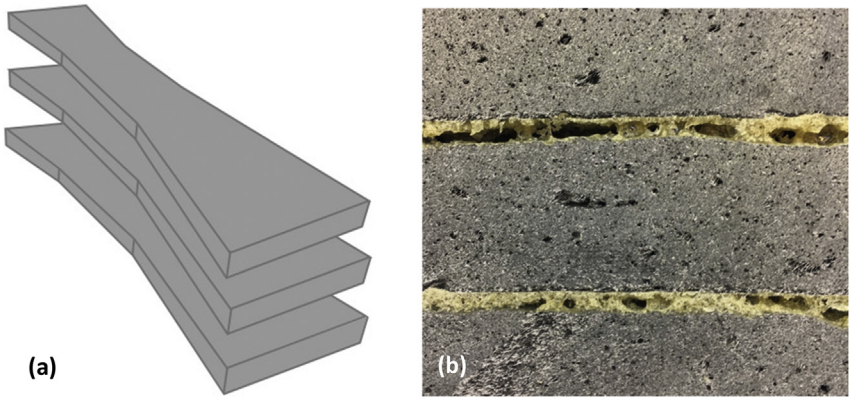

Fig. 3. (a) An exploded view of the primary layer orientation used for the stacked layering schemes' ("PU-bonded" and "Hybrid") tensile specimens. In the PU-bonded scheme, as seen in transverse cross-section in (b), PU adhesive are applied at the interfaces between the primary layers, while additional layers of HSHDC material are cast between pre-cast layers in the Hybrid scheme.

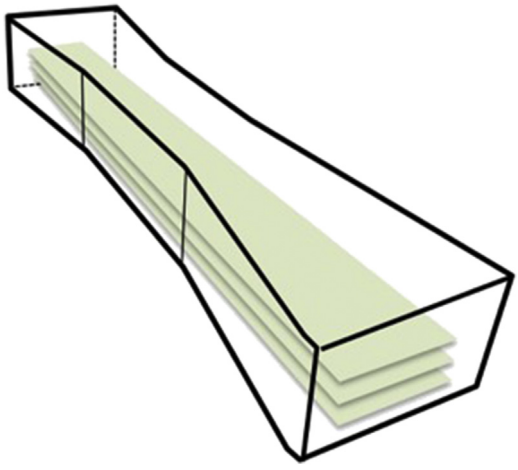

Fig. 4. Illustration of the orientation of three mesh layers within tensile specimens tested in this study. The number of mesh layers, which also dictates the total number of layers, is used as a variable.

Fig. 5. Opposing faces exposed after layer debonding and sectioning of a VCP-mesh specimen. Interlayer mineral bridges or pillars are formed through the mesh apertures and subsequently severed during loading, leaving a marked surface roughness that may contribute a desired resistance to layer sliding. Interfaces in the PP-mesh scheme have a similar appearance, but with larger mesh apertures and thus larger interlayer mineral pillars.

4. Results and discussion

Performance of the various schemes in tension, bending, and compression is presented and compared, followed by discussion of the effects of structuring features on deformation mechanisms, failure modes, and overall mechanical performance.

4.1. Performance in direct tension

The tensile strength and tensile strain capacities of each of the nacre-inspired composite design schemes are compared in Fig. 7.

The relative parity amongst these tensile strength results indicate that composite tensile strength remains highly dependent on cementitious matrix strength and fiber bridging capacity, just as in unstructured (monolithic) ECC. The various nacre-inspired schemes do not appear to significantly alter ultimate strength at this size scale, with the exception of the prestrained PU-bonded scheme, which suffers reduced strength due to the damage accumulated in the HSHDC material during the prestraining process.

occurrence of natural casting flaws, inflating both strain capacity and ultimate tensile strength. The larger, square cross section of the large dogbone specimens used for tensile characterization here more accurately measures how cementitious material would perform in full-scale, structural applications using full-scale casting methods.

4.2. Performance in flexure

The advantages of the nacre-inspired structuring schemes are more apparent in flexure (Fig. 8). All schemes tested, with the exception of the PU-bonded scheme, show at least a 30% increase in modulus of rupture. The PP-mesh schemes demonstrate the best performance in bending with an approximately 100% increase in modulus of rupture, in combination with a dramatic improvement (up to 6×) in inelastic flexural toughness.

The improvement in flexure seen in the nacre-inspired schemes is not surprising when it is considered that natural nacre is specifically meant to lend flexural toughness to the shells in which it is found. The shells in which nacre is seen generally have an extremely hard outer mineral layer, while nacre coats the inside of the shell, primarily to protect against bending moments and through-cracking generated in the case of highly concentrated loads or impacts.

The nacre-inspired schemes tested here illustrate a range of performance profiles. The PP-mesh schemes demonstrate the combination of significant increases in both flexural strength and flexural toughness, while the PU-bonded scheme proves to be an option for prioritizing high energy absorption/dissipation over high strength.

The hybrid pre-cast/cast-in-place scheme was previously tested in flexure, and showed improved inelastic flexural toughness compared to monolithic HSHDC [22]. However no significant improvements in modulus of rupture were observed in flexure, unlike in the mesh schemes.

The weak interfaces in the PP-mesh WD40 (3-layer) scheme do not appear to negatively affect performance in flexure, indicating that the bond between the PP-mesh and the cementitious matrix is already inherently weak and does not play a significant role in composite performance.

The PP-mesh schemes outstrip the VCP schemes in flexure performance. This discrepancy is discussed in Section 4.4. With the cost of PP-mesh being relatively low compared to that of the VCP mesh, the PP-mesh schemes are the most promising of those tested in this study based on both tensile and flexural performance.

Initial flexural stiffness (elastic) is also considered. The monolithic scheme exhibits the highest stiffness (24.4 MPa/mm), while the PU-bonded scheme (4 HSHDC layers) exhibits the lowest of the schemes tested in flexure (9.2 MPa/mm). The PP-mesh WD40 scheme had the highest average initial elastic stiffness of the nacre-inspired schemes at 17.89 MPa/mm. Within each scheme, an increase in the number of total layers (primary + secondary) was generally correlated with a reduction in initial flexural stiffness.

4.3. Performance in compression

As the most promising nacre-inspired scheme in tension and flexure, the PP-mesh scheme is compared to monolithic HSHDC in compression. The PP-mesh composite scheme is tested in two orientations: with the mesh and HSHDC layers oriented normal to the loading axis and parallel to the loading axis. As seen in Fig. 9, the PP-mesh scheme demonstrated consistently higher

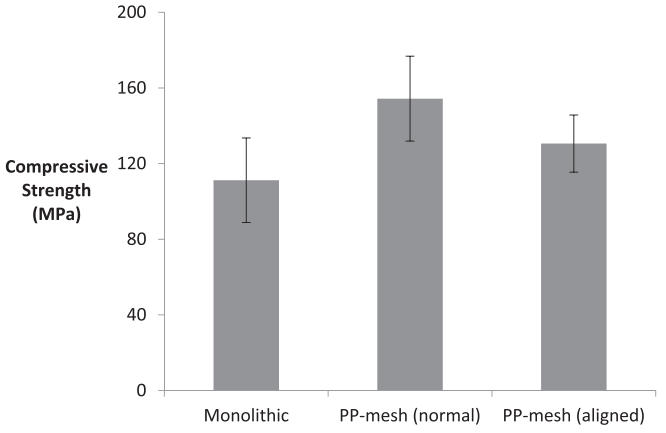

Fig. 9. The performance in compression of the PP-mesh nacre-inspired scheme is compared with that of the monolithic HSHDC case at an age of 14 days.

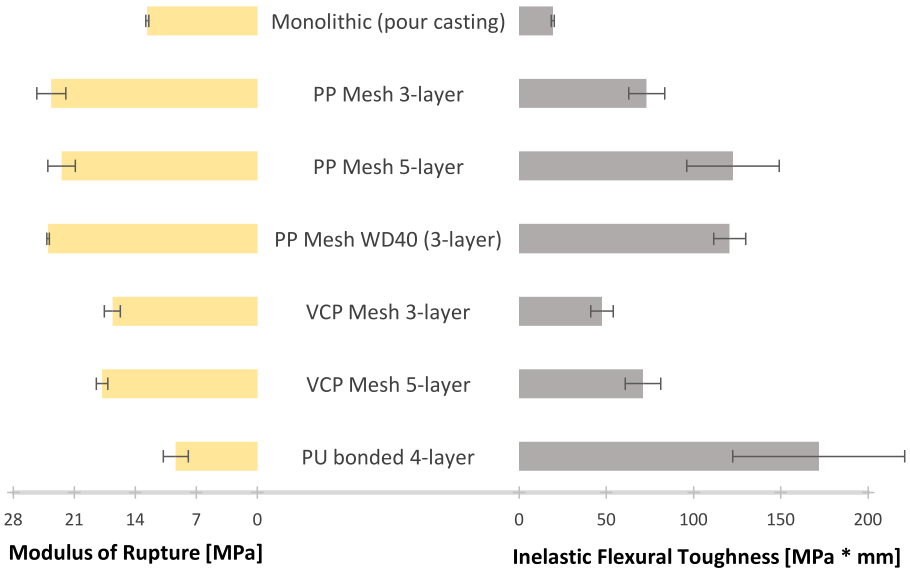

Fig. 8. Modulus of rupture and inelastic flexural toughness are of various nacre-inspired composite design schemes are compared.

compressive strength, in both orientations, than the monolithic case.

The mesh component's contribution to improved performance in compression can probably be attributed to deformation mechanism manipulation. In tension the mesh layers may carry some tensile load, acting as “reinforcement”, but in compression, the mesh would not be contributing to load carrying capacity. Instead, performance enhancement is likely a result of crack paths within the HSHDC layers being altered by the mesh layers, dissipating energy and suppressing failure via layer debonding and crack bifurcation in both orientations.

This improvement in compressive performance is not necessarily expected as nacre has not been seen to exhibit higher compressive performance than bulk aragonite.

It should be noted that monolithic HSHDC has been previously reported to have an average compressive strength of ~160 MPa [23], similar to what is measured here for the PP-mesh scheme (normal orientation). Using the control series benchmark (monolithic series) from this study, however, it appears clear that the nacre-inspired schemes, designed to improve tensile and flexure performance, also offers a boost in compressive strength. Using specimens prepared as part of the same study provides a more direct method of comparison and eliminates other factors that may be the source of this quantitative discrepancy in performance.

4.4. Effect of material structuring on deformation mechanisms, damage progression, and failure modes

Observation of cracking patterns and deformation progression suggests that nacre-inspired deformation mechanisms are being generated within the nacre-inspired composite schemes and may be associated with strain capacity and modulus of rupture improvements over the monolithic case.

4.4.1. Compartmentalization of damage

One mechanism contributing to the nacre-inspired schemes' boost in tensile strain capacity, modulus of rupture, and inelastic flexural toughness appears to be the ability of the layered specimens to isolate an accumulation of damage within each primary layer, at least to a degree. The HSHDC material, upon which the various layering schemes are based, inherently suppresses failure by distributing damage throughout the material instead of allowing damage to localize at a single weak point. However, this material is only able distribute damage in one dimension (the length of the gage section of the tensile specimen or length of the span in flexure). The layered nacre-inspired hierarchical composites are able to distribute damage along the length of the gage/span section, but also between different primary layers, which, in some cases, are able to contain the damage without affecting other layers.

This compartmentalization of damage within layers is observed in every one of the nacre-inspired design schemes tested here, but through cracking behavior is not necessarily excluded. Compartmentalization is evident when cracks are arrested or caused to bifurcate at the mesh interlayer boundary. Based on the observed occurrence of crack arrest, it is an initial layer debonding at the secondary layer interface that promotes this compartmentalization. Several instances of layer debonding and crack arrest are seen in the longitudinal cross-sections of tensile specimens shown in Fig. 10. In other instances, also seen in Fig. 10, cracks appear to be contained, not within one layer, but within two or three adjacent layers. This behavior is similar to process zones that appear in nacre under extreme loading, as seen in Wang et al. (2001) and Kakisawa and Sumitomo, (2012) [4,5]. The appearance of the longitudinal cross sections of the PP-mesh and VCP specimens in Fig. 10 can be compared to that of the monolithic specimen pictured in Fig. 11, which shows a much higher degree of through cracking.

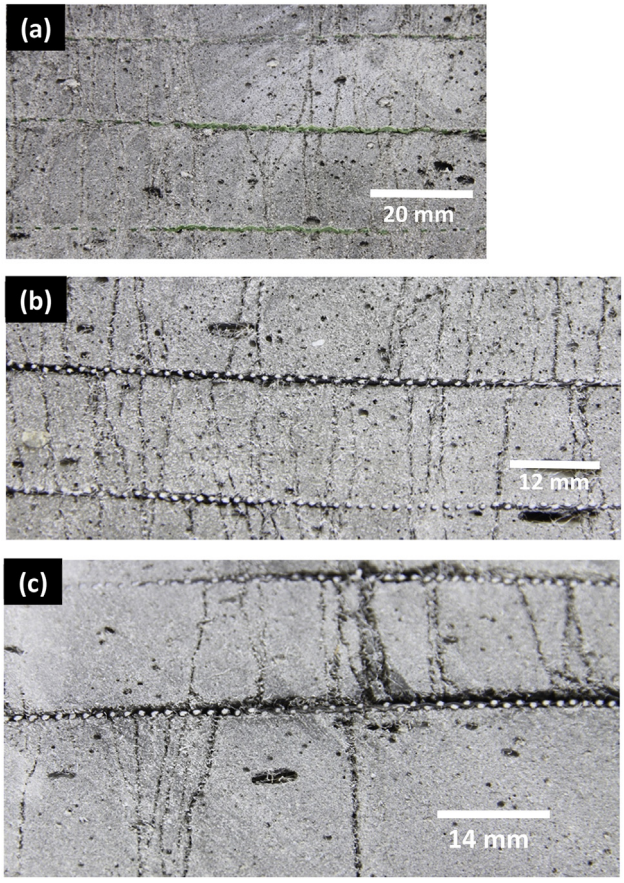

Fig. 10. Longitudinal cross sections of the PP-mesh (a) and VCP-mesh (b and c) layering schemes tested in direct tension, showing the containment of damage (cracking) either within a layer or within several adjacent layers.

In addition to the observed instances of crack arrest between primary layers, compartmentalization of damage within layers in the PP-mesh scheme is also indicated by the cracking observed parallel to the loading direction. In Fig. 12, a progression of damage accumulation in a single specimen shows multiple longitudinal cracks developing parallel to the loading direction (up and down, as pictured). These cracks correspond to the locations of PP-mesh interlayers within the specimen and indicate that shear stress is occurring at the interlayer boundaries as damage accumulates in each layer at different rates.

In the PP-mesh scheme, fewer layers are employed than in nacre

Fig. 11. A longitudinal cross section of a monolithic scheme tensile specimen showing a high degree of complete through-cracking.

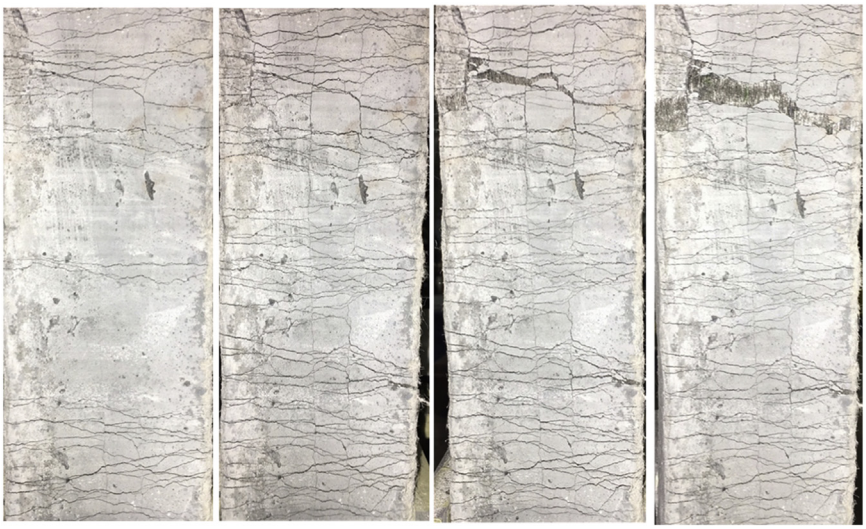

Fig. 12. Progression of damage (from left to right) in a single PP-mesh tensile specimen, showing the development of several longitudinal cracks, parallel to the loading direction (vertical), corresponding with locations of PP-mesh within the specimen. (Scale: the specimen pictured has a horizontal width of ~76 mm).

due to processing and cost constraints, but the principal is preserved: multiple layers allow damage to not only be distributed, but also compartmentalized, to a higher degree than a monolithic case, contributing to the improved macroscopic performance.

4.4.2. Layer sliding and resistance to sliding

The vertical cracks and large failure crack seen in the last image of the progression shown in Fig. 12, show evidence of layer sliding, related to the accumulation of damage within each layer at different rates. The left most layer (as pictured in Fig. 12) has slid significantly relative to the adjacent layer near the location of failure. It is seen that the failure crack has a tortuous path, influenced by the layering scheme.

Layer sliding is part of a deformation mechanism in nacre that generates local slip-hardening, and macroscale damage distribution, strain-hardening, tensile ductility, and enhanced material toughness. The microcracks generated within each of the primary HSHDC layers are analogous to the “activation sites” produced in nacre when tablets slide relative to those adjacent. Each of these features, microcracking and tablet activation, provides a “give” within the material and are spread throughout the material instead of localizing. To generate the necessary slip-hardening behavior, however, there must be some interlayer resistance to sliding, once it has been initiated.

Intralayer resistance is provided in part by the fibers bridging the microcracks within each layer, analogous to the organic bridging in nacre (depicted in Figure A1). Of course, in nacre tablets are pre-defined via the growth process, and in the PP-mesh scheme, the discrete units are generated under loading via microcracks. However, the activation of these sites, resistance to continued sliding, and distribution of damage occur in similar ways in both nacre and the PP-mesh nacre-inspired scheme.

Additional interlayer resistance to sliding is also required to suppress intralayer failure as stress continues to build. In the mesh schemes, the layer waviness and surface roughness left by the severed mineral pillars was hypothesized to contribute to interlayer sliding resistance, but why do the PP-mesh schemes outperform the VCP-mesh schemes in flexure, where layer debonding and sliding occur more readily? The answer could be the small number of polymer fibers that pass through the PP-mesh and connect adjacent layers through the mineral pillars formed in the mesh apertures, as pictures in several PP-mesh specimens in Fig. 13. These exposed fibers, indicating evidence of fiber pullout, are not seen in the VCP-mesh specimens, presumably because of the smaller aperture size.

The relative sparsity of these interlayer fibers compared to those available for intralayer crack bridging, as observed in the PP-mesh schemes, means that the interlayer bridging strength is relatively low, but the force required for pullout of these fibers still contributes resistance to layer sliding after the mineral pillars have been severed. These limited but consistently observed interlayer fibers serve a similar role to the interfacial biopolymer component in nacre, providing ligamental adhesion between layers and resistance to layer sliding.

The absence of interlayer fibers in the VCP specimens (Fig. 5), due to the smaller mesh aperture size, may be the reason the PP-mesh scheme outperforms the VCP schemes in flexure. The sliding distances between layers are greater in flexure than in direct tension, meaning the effect of the resistance to layer sliding is more pronounced between schemes. Despite layer delamination (and associated crack arrest and bifurcation) being observed with more consistency in VCP-mesh schemes than in the PP-mesh schemes, flexural performance of the VCP-mesh schemes lagged behind that of the PP-mesh schemes. While simply generating layer delamination in the composite offers benefits over the monolithic case, the importance of generating subsequent resistance to layer sliding is highlighted. The superior performance of the PP-mesh scheme suggests that the interlayer polymer fibers, playing the role of nacre's interfacial biopolymer, likely provide more effective sliding resistance than layer waviness and surface roughness in the large-scale, nacre-inspired composite schemes.

Layer sliding resistance is also observed in the PU-bonded schemes, as evidenced by elongated appearance of the adhesive remaining attached to either side of the HSHDC layer interface (Fig. 14). Friction generated between the rough, adhesive covered surfaces remaining after the strength or strain limit of the adhesive has been reached, likely also contributes in flexure where sliding distances are larger. Significant layer sliding distances (up to 5 mm) are observed in the PU-bonded bending specimens, which showed the largest deflections prior to failure, but inferior modulus of rupture to the monolithic case in flexure.

The sliding resistance provided by the PU adhesive, and the

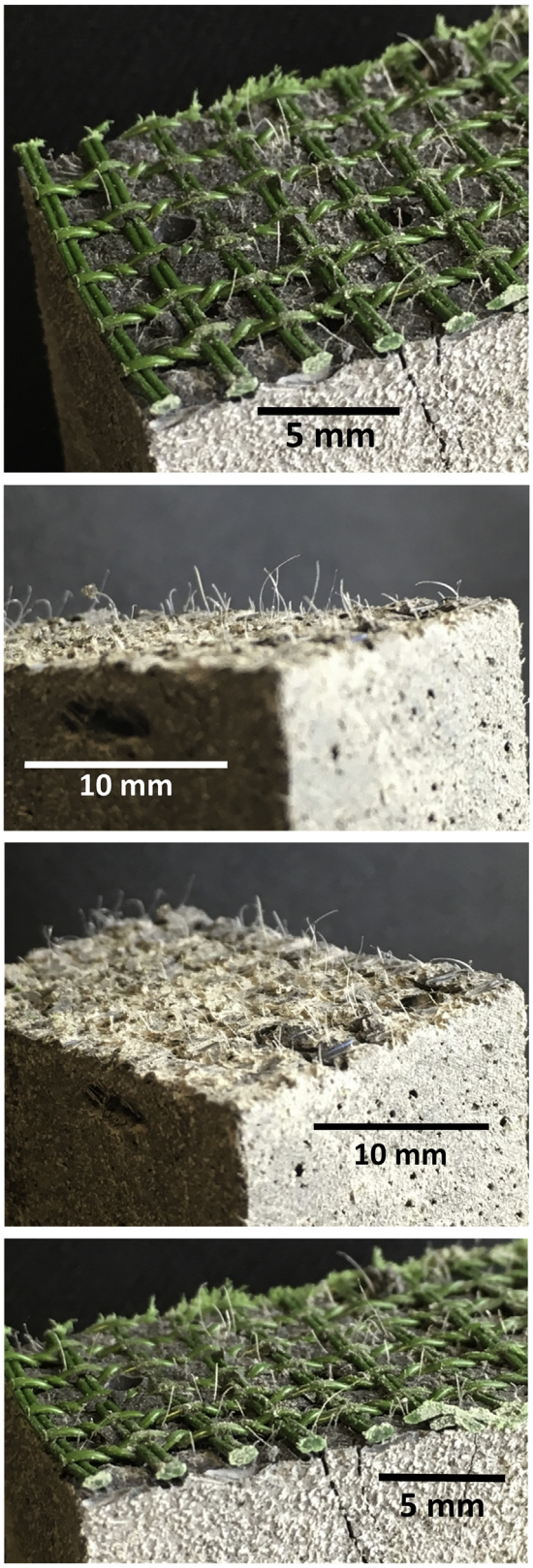

Fig. 13. Interlayer fibers are observed in the PP-mesh schemes when layers debonded during testing are sectioned and the interfacial surfaces are exposed. Interlayer fibers were not observed in the VCP-mesh (Fig. 6) scheme, nor in other nacre-inspired schemes.

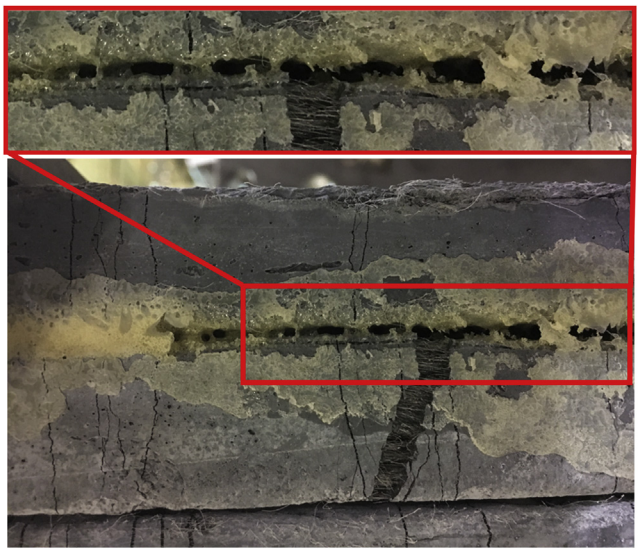

Fig. 14. An example of the elongation of the remaining interfacial adhesive (circled), in an area of a prestrained PU-bonded tensile specimen where layer sliding has taken place, suggesting a degree of HSHDC layer sliding resistance provided by the adhesive. Similar observations were made in other locations in the prestrained PU-bonded specimens.

sequence of forces are applied to the adhesive, may explain the significantly higher strain capacity of the prestrained PU-bonded scheme in direct tension compared to the other PU-bonded schemes. In the normal PU-bonded schemes, the sudden appearance of cracks at the high stresses carried by the HSHDC matrix (and bridging fibers) cause a high rate of shear loading upon the adhesive material, perhaps debonding locally around cracks suddenly, without contributing to load carrying capacity. In the prestrained PU-bonded schemes, the profile of loading upon the adhesive material is different. Because the HSHDC layers are already cracked at intervals along the gage section, tensile strain initially occurs at lower stresses and at a much more gradual, controlled rate. This allows the adhesive material, as shear forces are applied to it, to share some of the load as HSHDC layers strain at slightly different rates. Cohesive debonding in the adhesive occurs only after it has substantially contributed to layer sliding resistance. Frictional resistance may even contribute after this limit has been reached. In this way, a larger strain can be reached prior to the exhaustion of the strength limit of the HSHDC, even though that strength limit may have been reduced due to the damage caused by prestraining.

While many of the schemes show layer sliding, and the requisite resistance to said sliding, comparing the overall mechanical performance of the various schemes, it is easy to pick the PP-mesh schemes as the most effective in applying nacre-inspired deformation mechanisms to enhance composite performance.

4.4.3. Progressive failure

All of the nacre-inspired schemes, in both tension and flexure, exhibit progressive failure: the sequential failure of single layers, while other layers preserve high stress carrying capacity, rather than total specimen failure. Even though through cracking is observed in many instances in the nacre-inspired schemes, “through failure” is prevented in every case.

Failure of any one of the layers, typically due to the exhaustion of crack bridging capacity of fibers across one of the cracks, often represents the end of composite scale strain-hardening simply because there is a reduced amount of material by which stress can

be carried. However, the composite retains significant load carrying capacity as the significant damage accumulated by the failed layer has been compartmentalized and isolated from the other layers. An example of this behavior occurring in the PP-mesh bending specimens is illustrated in the sequence of images in Fig. 15. Similar occurrences were seen in every nacre-inspired scheme. While other layers have also accumulated damage to accommodate the strain levels required to cause the first layer to complete the fiber pullout/rupture process, they have been shielded from whatever weakness caused the loss of load carrying capacity in the failed layer. In this way, the composite can maintain a stress carrying capacity relatively close to its ultimate strength, even after significant damage has been accumulated and terminal stress decay has begun. This enhances composite toughness and provides a fail-safe mechanism. Such behavior is well suited to the critical applications in which a nacre-inspired cementitious building material could be justifiably deployed.

4.5. Continued development

While advantages of using nacre-inspired features and deformation mechanisms have been shown, continued development needs to address durability of such composite schemes in a variety of environmental conditions and under cyclic loading conditions.

Additionally, alternate routes to producing nacre-inspired features and deformation mechanisms remain to be explored. The layered structure of nacre is a natural fit for fabrication processing via the large-scale 3D printing techniques currently being pioneered for automated, additive manufacturing of full-scale structures. Similarly, the benefits of layered strain-hardening cementitious composites reported here, and previously in Soltan et al. (2014), have advantageous implications for structural members 3D printed using strain-hardening cementitious composite material [22].

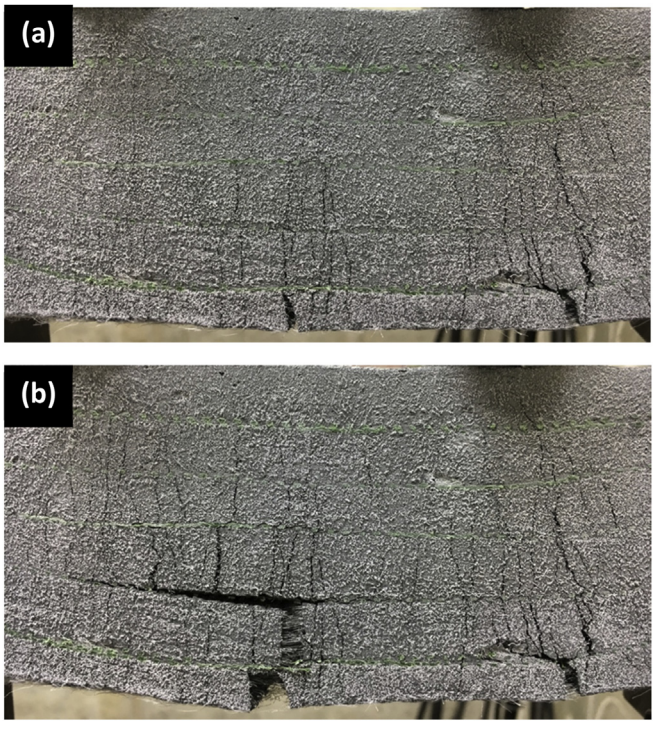

Fig. 15. An example of the progressive failure behavior is seen in the PP-mesh scheme under flexure. In (a) the bottom layer has failed while the remaining five layers carry the flexural stress. In (b) the new "effective bottom layer" (second from bottom) has failed, while the remaining four retain load carrying capacity. The significant damage accumulated in the most tensile (bottom) layers is isolated from the upper layers, suppressing total failure of load carrying capacity.

5. Conclusions

Approaches to adapting features and associated deformation mechanisms of nacre to a larger size scale and in materials applicable to civil infrastructure have been investigated. Various nacre-inspired hierarchical composite designs, based on strain-hardening cementitious composites, are evaluated in direct tension and flexure. The following conclusions can be drawn from this work:

The nacre-inspired composite design schemes tested herein, adapted to a much larger size scale than that of nacre, can provide strain-hardening cementitious composites significantly enhanced modulus of rupture (stress carrying capacity) and inelastic flexural toughness in flexure. In direct tension, significant benefits are seen for tensile strain capacity, but any improvements in tensile strength are small, and in several of the nacre-inspired composite schemes improvements in strain capacity come at the expense of tensile strength.

Both the "stacked layer" and "mesh layer" schemes show improvements in mechanical performance, however, the mesh schemes provide more consistent performance and property profiles better suited structural applications in which strength is prioritized over capacity for deformation prior to failure.

Of the schemes tested in this study, the mesh schemes incorporating polypropylene (PP) mesh, with aperture size of 6.25 mm^2, provide the best overall mechanical property benefits and outperforming other mesh schemes with smaller aperture sizes. While all the mesh schemes incorporated distinct layers, interlayer mineral pillars, interfacial surface roughness (after pillar fracture), and nested waviness (all features inspired by nacre's structure), the interlayer fibers allowed by the larger mesh apertures in the PP mesh appeared to provide the most effective resistance to layer sliding, resulting in the best performance in flexure, where layer sliding is most pronounced. The interlayer fibers, in the PP-mesh schemes behave as an analog to the interfacial biopolymer in natural nacre, providing ligamental adhesion between layers and allowing controlled sliding (shear) between primary layers.

In addition to enhanced tensile strain capacity, tensile strength, modulus of rupture, and inelastic flexural toughness, the PP-mesh scheme also exhibited enhanced compressive strength compared to the monolithic form of its primary material, HSHDC. This enhanced compressive performance of the hierarchical composite over the primary component is not observed in natural nacre.

Layer debonding is observed in all the nacre-inspired schemes tested in this study and contributes to compartmentalization of damage. Layer debonding, itself an energy dissipation mode, gives rise to crack arrest and crack bifurcation, which also contribute to fracture suppression.

Progressive failure, in which total composite failure is suppressed by virtue of intralayer compartmentalization of damage, provides a failsafe feature to all nacre-inspired design schemes presented here. This feature is particularly applicable to the critical use cases—such as seismic, impact, and blast resistance—in which enhanced strength, strain capacity, and toughness of cementitious materials already offer a value proposition.

Funding

This work was supported by the University of Michigan through the MCubed program.

Acknowledgements

The authors thank Bob Spence and Jan Pantolin for instrument maintenance and technical support, Bob Fischer for machining and guidance in the fabrication of grips for the large dogbone tensile testing apparatus, Prof. Ravi Ranade for initial project guidance and HSHDC material development, Prof. Nima Rahbar for discussions regarding structural features and slip-hardening mechanisms of natural nacre, Lafarge for donation of Class H cement, Elkem for donation of Microsilica, and the University of Michigan MCubed cross-disciplinary research funding program for supporting and encouraging innovative, multi-disciplinary collaborative research.

Appendix A. Supplementary data

Supplementary data related to this article can be found at https://doi.org/10.1016/j.cemconcomp.2018.02.006.

Appendix I. HSHDC compositional information

Presented here is additional information regarding the materials used in the cementitious composites reported in this study. Quantitative information presented in this appendix was provided by the materials' respective manufacturers/suppliers. Additional discussion of this composition can be found in Ranade et al. (2011) [24].

Microsilica: Elkem 955 undensified Microsilica (silica fume)

Table I
1: Chemical composition of Elkem Microsilica (Silica Fume) Grade 955 (undensified)

Compositional Component	Content (%)
SiO_2	95.5 (min)
C_{free}[b]	1.0 (max)
Fe_2O_3	0.3 (max)
Al_2O_3	1.0 (max)
CaO	0.4 (max)
MgO	0.5 (max)
K_2O	1.0 (max)
Na_2O	0.4 (max)
H_2O[a]	1.0 (max)

[a] When packed.
[b] C in SiC not counted.

Class H cement: The primary cementitious component used is Lafarge Class H oil well cement.

HRWRA: The high range water reducing admixture used is W.R. Grace ADVA 190, a polycarboxylate superplasticizer.

Ground Silica: US Silica brand Sil-Co-Sil 75 (crystalline quartz).

F-60 silica sand: US Silica brand F-60 silica sand.

UHMW-PE Fiber: The ultra high molecular weight polyethylene fibers used is Honeywell brand Spectra 900 (675 denier), cut to 0.5" (12.7 mm) by Minifibers, Inc. (Johnson City, TN). The fibers have a diameter of 38 microns, a niminal strength of 3000 MPa, modulus of 100 GPa, and specific density of 0.97.

Appendix II. –HSHDC mixing and accelerated curing procedure

A 12 gallon Hobart planetary style mixer is used. Dry ingredients (excluding fibers) are first mixed for at least 5 min, then approximately one third of this dry mix is removed from the mixer to be added in later in small amounts at regular time intervals to aid proper hydration and mixing. The entire water content is added at time, t = 0. The HRWRA content is added immediately after the addition of water at approximately t = 30 s. Over the next several minutes the mix turns from a damp powder to liquefied paste. At this point the remainder of the dry mix is reintegrated in several steps. The mix is allowed to return to a paste-like state prior to the addition of more of the dry mix. Prior to fiber addition, half of the fiber content (by weight) is first soaked in water for several minutes. The water (as much as possible) is then wrung out of this portion of fibers via manual squeezing. The fibers are reweighed to determine the additional water content being added to the mix. The additional water carried by the soaked portion of the fibers when added to the mix is approximately 0.38–0.45 g water for 1.0 g of total fibers (dry weight). Once all the dry ingredients have been thoroughly mixed into the paste, fibers are added in small handfuls, with clumps of the soaked fibers picked apart by hand prior to being added. The vinyl-silane coupling agent is added immediately fiber addition is completed. Mixing is continued for 2–3 min after the addition of the coupling agent. Casting is then performed immediately.

Demolding is performed 24–48 h after casting (depending on size of specimen). Specimens are then placed in a room temperature water bath for seven days for continued hydration. Specimens are then placed in an elevated temperature (80C) water bath for four additional days, after which they are removed from the water bath and dried at elevated temperature (70–80C) for at least 24 h. Specimens are allowed to return to room temperature prior to testing. In schemes where polymer adhesive is applied following this curing process, the adhesive is allowed to cure for an additional 4–5 days.

Appendix III. –Nacre-inspired composite design philosophy, approaches, and descriptions

Several design schemes are explored to incorporate nacre-inspired features associated with the key deformation mechanisms observed in nacre, on a scale and in a material applicable for full-scale construction and infrastructure.

All the design schemes reported here use the specific compositional version of ECC developed by Ranade et al. (2013) and described in Section 2.1, which has been previously reported to have high compressive strength, high tensile strength, and high strain capacity (i.e ductility) [23]. This high strength ECC, called HSHDC, forms what are hereafter referred to as "primary layers" within the various nacre-inspired design schemes.

The HSHDC material is not a direct analog to the aragonite material found in nacre. Aragonite is inherently brittle and weak in the bulk state. The HSHDC material is composed of a densified, high strength cementitious matrix, which could be thought of similarly to the high strength exhibited by the microscale aragonite tablets, but also includes 12.7 mm long, 38 micron diameter ultra-high molecular weight polyethylene fibers. These high tenacity polymer fibers do not have a direct analog in the nacre structure, however, they allow the segmentation of the HSHDC cementitious matrix material under tensile stress that approximates the tablet structure of nacre. As the cementitious matrix undergoes multiple cracking under tensile stress, the polymer fibers also provide a resistance to further deformation, similarly to the ligamental biopolymer connections between tablets within the same layer in natural nacre (Figure A1).

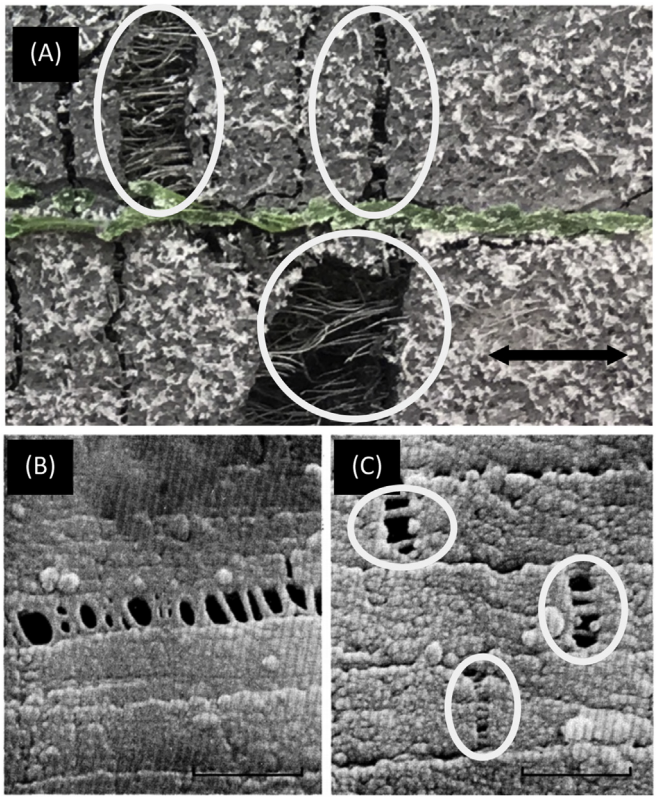

Fig. A1. The crack-bridging fibers in HSHDC (circled in A) contribute to strain hardening behavior in the material, similarly to the biopolymer component between intralayer tablets (circled in (C)) in nacre. The biopolymer component between layers in nacre (B) inspires several other analog features in the structural composites investigated in this study. Scale bars: (A) = 8 mm, (B) and (C) = 0.60 microns [(B) and (C) adapted from A.P. Jackson et al., 1988 (Proc. R. Soc. Lond. B)].

These nacre-inspired composite designs, based on the ECC material system are not meant to be direct mimics of nacre's structure, but instead interpretative adaptations of the structure being realistically applicable to large scale construction applications. It is the generation of nacre-inspired deformation mechanisms, on a larger size scale, that is prioritized and targeted for investigation.

There are two main approaches to the physical adaptation of nacre's structure and deformation mechanisms to a large-scale structural material reported here. The first is stacking multiple layers of precast ECC in various ways and manipulating the interface between the layers. The second approach is creating distinct layers within the cementitious composite via inlayed mesh materials. Each approach incorporates approximations of key features seen in nacre through different processing and compositional routes.

The compositional constituents and processing steps explored have been deemed to be feasible within the realistic constraints of large scale construction. While these design schemes have been devised be realistic for actual large-scale application, the forms in which they are presented are meant to serve simply as simplified physical models of various nacre-inspired design strategies and have not been optimized. There remain several parameters for each design scheme that could be further tuned to manipulate mechanical performance, cost, and other application specificity.

These physical models are used to determine the potential mechanical utility of nacre-inspired design features in cementitious material systems on a size scale much larger than that of natural nacre. To determine these effects, the nacre-inspired schemes are compared to the monolithic version of the same ECC material that serves as the primary component of all the nacre-inspired design schemes. The composite design schemes investigated herein are summarized in Table 2.

Monolithic control scheme

Two version of the monolithic control series are tested. The first is monolithic specimens formed via freshly mixed HSHDC material being poured into molds, similarly to how the material would be processed and shaped for real, large-scale applications.

The second version of the monolithic HSHDC control uses a more refined casting process in which molds are filled in a stepwise manner, such that the discontinuous fibers within the HSHDC are allowed to preferentially align in the planar orientation normal to mold filling direction. This creates fiber alignment (in a planar orientation, rather than unidirectional), without the formation of discrete layers like those intentionally created in the nacre-inspired schemes. This control series can help isolate the effect of intentionally weak interfaces within the nacre-inspired schemes from that of simple 2D fiber alignment.

Stacked layering design schemes

This group of design schemes uses precast HSHDC layers (primary layers) stacked in a variety of manners and with a variety of interfacial secondary layers between. The orientation of these layers in the large, dog-bone shaped tensile specimens is illustrated in Fig. 3 (a).

The adhesive interface scheme uses a commercially-available, high strength polyurethane adhesive as an analog to the biopolymer interfacial layers within nacre. The biopolymer in nacre is characterized as (1) having extremely high strength of adhesion to the mineral tablets, (2) allowing sliding of tablets relative to each other while, and (3) maintaining ligamental attachment to tablets during sliding, providing mechanical resistance to continued sliding. This particular polyurethane adhesive was chosen using this criteria. A transverse cross section of this scheme, hereafter referred to as the “PU-bonded scheme”, is seen in Fig. 3 (b).

A styrenic block copolymer exhibiting ligamental attachment in shear and tensile loading arrangements was also explored during preliminary testing, but did not perform as well as the polyurethane adhesive due to lower strength of adhesion to the cementitious material and limited resistance to layer sliding.

Prestraining of the pre-cast layers, to generate discrete segments within the HSHDC material, prior to application of the PU adhesive is also investigated. This scheme, labeled as “Prestrained PU-bonded” is meant to more closely mirror the structure of nacre in that the segmented structure within each layer is present prior to the application of excessive loading. To produce these specimens, the primary layers, like those depicted in Fig. 3(a), are individually subjected to uniaxial tension and bidirectional bending forces to generate well-distributed microcracking throughout. Bidirectional bending entails subjecting a specimen to four point bending (below its maximum stress capacity), unloading specimen, flipping it upside down, and subjecting it to bending again, this time in the other “direction”. All cracks generated in the primary layers are oriented perpendicular to the eventual tensile loading direction in the large dogbone composite specimens. The degree of prestrain applied to each layer is kept below the average strain capacity of typical, high aspect ratio (thin layer) HSHDC specimens (2–3% pre-strain). This level of prestrain was chosen based on previous experience with thin layer HSHDC specimens and represents an intermediate between the competing factors of well-distributed microcracking and

retained strength of the specimen. After unloading, the layers are adhered together with the PU adhesive and a constant force is applied to promote the quality of bonding and mitigate the natural expansion of the PU bondlines, just as in the other PU-bonded schemes.

An additional stacking scheme, alternating precast layers with freshly cast layers with no additional interfacial component as described in Soltan et al. (2014) [22], was also investigated. In this scheme, referred to hereafter as the “Hybrid” scheme, the natural surface roughness on the precast layers contributes to an interfacial bond formed between the precast and cast-in-place layers, which is intentionally weak. With no fibers bridging across these interfaces within the composite, layers are allowed to deform independently under excessive loading after the initial bond is severed, hypothetically promoting crack arrest, energy dissipation, and compartmentalization of damage.

This Hybrid scheme was observed to have fewer internal voids at the interfaces than the PU-bonded stacked schemes. As seen in Fig. 3(b), significant voids are present between stacked primary layers in the PU-bonding scheme due to non-flat surfaces of the pre-cast primary layers, as well as naturally occurring air entrapment in the foaming PU adhesive during curing.

The thickness of the primary layers in the stacked scheme specimens depends upon on the number of total cementitious layers in the scheme. The total thickness of the composite tensile specimens was kept at ~76 mm regardless of scheme. The hybrid scheme includes four layers (two precast, two cast in place), and both 3 and 4 primary layer specimens were tested in tension for the PU bonded scheme.

Mesh layering design schemes

Polymer meshes were used as an alternate approach to create nacre-inspired structures and deformation mechanisms. In these schemes the secondary layers are polymer mesh materials, and they not only act as the interface between primary HSHDC layers, but they serve to distinguish and shape the primary layers during initial composite fabrication. During casting, mesh layers are alternated with cementitious material during mold filling to create a layered structure. Fig. 4 illustrates the orientation of mesh layers (depicted in green) within the dogbone shaped tensile specimens, aligning with the loading direction. The same orientation is used for the beam specimens, but in flexure, the loading direction is normal to the planar orientation of the mesh and HSHDC layers.

Two mesh materials are used in this investigation and the number of mesh layers is used as a variable. Regardless of number, the mesh secondary layers are spaced relatively evenly through the thickness of the composite, manipulating the thickness of the primary cementitious layers.

The alternating fiber-reinforced cementitious material and polymer meshes mimic nacre's structure in a number of ways. First, the meshes create distinct layers of cementitious material. The fibers within the cementitious material are generally confined to a single layer, creating intentionally weak interfaces between cementitious layers without fiber bridging, and strengthening each layer because of enhanced intra-layer fiber alignment. The meshes also create pillars of cementitious material between cementitious layers due to the apertures in the mesh. This is analogous to the mineral pillars observed in nacre that provide initial stiffness. Just as in nacre, these “pillars” are more susceptible to fracturing in shear and tension than the cementitious layers and are severed under extreme loading. After the pillars are severed under loading, the material remaining attached to each cementitious layer acts as a roughened surface (see Fig. 5) to provide enhanced resistance to shearing/sliding between layers. Additionally, these mesh layers are cast into the composite so as to impart a wavy shape to the cementitious layers, while allowing contiguous layers to nest into each other (see Fig. 6), just as in nacre. This waviness in nacre is thought to contribute to strain and shear-hardening behavior that enhances nacre's toughness. By capturing the essence and hypothesized functionality of the interlayer mineral pillars, interfacial surface roughness, and wavy, nested shaping of the layers, all three of the mechanisms previously proposed to be responsible for nacre's resistance to layer sliding are incorporated in the layered mesh approach [1,4,5,7,9,25–27].

Additional benefits of this mesh-based structuring approach were observed during mechanical testing and are discussed in Section 4.3.

To determine the reinforcing contribution of the mesh to tensile and flexural performance, a scheme with purposefully weak interfaces is also tested. In this scheme, called “PP-mesh WD40”, mesh layers are coated in mold release (WD40) prior to being cast into the tensile and beam bending specimens. By discouraging bonding between the polymer mesh and the cementitious matrix, the contribution of the structuring allowed by the mesh, rather than the mesh as a reinforcement per se, can be shown more clearly. Similarly, the monolithic scheme with aligned fibers is also meant to provide context to the performance of the layered mesh schemes regarding textile reinforcement contributions.

References

[1] F.H. Barthelat, P.D. Tang, C.-M. Zavattieri, Li, H.D. Espinosa, On the mechanics of mother-of-pearl: a key feature in the material hierarchical structure, J. Mech. Phys. Solid. 55 (2) (2007) 306–337.

[2] F. Barthelat, J. Rim, H.D. Espinosa, A review on the structure and mechanical properties of mollusk shells - perspectives on synthetic biomimetic materials, in: B. Bhushan, H. Fuchs (Eds.), Appl. Scanning Probe Methods XIII, Springer, 2009, pp. 1059–1100.

[3] M.S. Davidson, Towards an Understanding of the Role of Aragonite in the Mechanical Properties of Nacre, PhD diss., Harvey Mudd College, 2009.

[4] H. Kakisawa, T. Sumitomo, The toughening mechanism of nacre and structural materials inspired by nacre, Sci. Technol. Adv. Mater. 12 (6) (2011), 064710.

[5] R.Z. Wang, Z. Suo, A.G. Evans, N. Yao, I.A. Aksay, Deformation mechanisms in nacre, J. Mater. Res. 16 (9) (2001) 2488–2493.

[6] F. Barthelat, H.D. Espinosa, An experimental investigation of deformation and fracture of nacre-mother of pearl, Exp. Mech. 47 (3) (2007) 311–324.

[7] M. Meyers, P. Chen, A. Lin, Y. Seki, Biological materials: structure and mechanical properties, Prog. Mater. Sci. 53 (1) (2008) 1–206.

[8] A.P. Jackson, J.F. Vincent, R.M. Turner, The mechanical design of nacre, Proc. Roy. Soc. Lond. B 234 (1988) 415–440.

[9] A. Evans, Z. Suo, R.Z. Wang, I.A. Aksay, M.Y. He, J.W. Hutchinson, Model for the robust mechanical behavior of nacre, J. Mater. Res. 16 (9) (2001).

[10] U.G.K. Wegst, H. Bai, E. Saiz, A.P. Tomsia, R.O. Ritchie, Bioinspired structural materials, Nat. Mater. 14 (2015) 23–36.

[11] F. Barthelat, Biomimetics for next generation materials, Phil. Trans. R. Soc. A 365 (2007) 2907–2919.

[12] P. Podsiadlo, S. Paternel, J.M. Rouillard, Z. Zhang, J. Lee, J.W. Lee, E. Gulari, N.A. Kotov, Layer-by-Layer assembly of nacre-like nanostructured composites with antimicrobial properties, Langmuir 21 (2005) 11915–11921.

[13] P.M. Hunger, A.E. Donius, U.G. Wegst, Platelets self-assemble into porous nacre during freeze casting, J. Mech. Behav. Biomed. Mater. 19 (2013) 87–93.

[14] A. Finnemore, P. Cunha, T. Shean, S. Vignolini, S. Guldin, M. Oyen, U. Steiner, Biomimetic layer-by-layer assembly of artificial nacre, Nat. Commun. (2012), https://doi.org/10.1038/ncomms1970.

[15] J.E. Rim, P.D. Zavattieri, A. Juster, H.D. Espinosa, Dimensional analysis and parametric studies for designing artificial nacre, J. of the Mech. Behav. of Biomed Mater. 4 (2) (2011) 190–211.

[16] H. Espinosa, A. Juster, F. Latourte, D. Gregoire, O. Loh, P. Zavattieri, Tablet-level origin of toughening in abalone shells and translation to synthetic composite materials, Nat. Commun. 2 (2011) 173.

[17] American Society of Civil Engineers, Report Card for America's Infrastructure, 2017. July 31, 2017, http://www.infrastructurereportcard.org/.

[18] R.F. Chandler, Life-cycle Cost Model for Evaluating the Sustainability of Bridge Decks: a Comparison of Conventional Concrete Joints and Engineered Cementitious Composite Link Slabs, A report of the Center of Sustainable Systems, University of Michigan, 2004.

[19] V.C. Li, On engineered cementitious composites (ECC): a review of the material and its applications, J. Adv. Concr. Technol. 1 (3) (November 2003) 215–230.

[20] V.C. Li, E. Herbert, Robust self-healing concrete for sustainable infrastructure,

J. Adv. Concr. Technol. 10 (2012) 207–218.
[21] M. Şahmarana, V.C. Li, Durability of mechanically loaded engineered cementitious composites under highly alkaline environments, Cement Concr. Compos. 30 (2) (February 2008) 72–78.
[22] D.G. Soltan, R. Ranade, V.C. Li, A bio-inspired cementitious composite for high energy absorption in infrastructural applications, in: Proc. Of the 13th Int. Symp. Multiscale, Multifunctional and Funct. Graded Mater., Blucher Material Science Proceedings, vol. 1, Blucher, São Paulo, 2014, pp. 1–4 n.1.
[23] R. Ranade, V.C. Li, M.D. Stults, W.F. Heard, T.S. Rushing, Composite properties of high-strength, high-ductility concrete, ACI Mater. J. 110 (4) (2013) 413–422.
[24] R. Ranade, M.D. Stults, V.C. Li, T.S. Rushing, J. Roth, W.F. Heard, Development of a high strength high ductility concrete, in: Proc. 2nd Int. RILEM Conf. Strain Hardening Cementitious Composites, Rio De Janiero, Brazil, 12–14 Dec, 2011.
[25] F. Barthelat, C.M. Li, C. Comi, H. Espinosa, Mechanical properties of nacre constituents and their impact on mechanical performance, J. Mater. Res. 21 (8) (2006) 1977–1986.
[26] F. Song, A.K. Soh, Y.L. Bai, Structural and mechanical properties of the organic matrix layers of nacre, Biomater. 24 (20) (September 2003) 3623–3631.
[27] K.S. Katti, D.R. Katti, S.M. Pradhan, A.P. Bhosle, Platelet interlocks are the key to toughness and strength in nacre, J. Mater. Res. 20 (5) (2005) 1097–1100.
[28] A. Peled, A. Bentur, Fabric structure and its reinforcing efficiency in textile reinforced cement composites, Comp.: Part A 34 (2003) 107–118.
[29] A. Brückner, R. Ortlepp, M. Curbach, Textile reinforced concrete for strengthening in bending and shear, Mater. Struct. 39 (2006) 741.
[30] H. Pakravan, M. Jamshidi, M. Latifi, M. Neshastehriz, Application of polypropylene nonwoven fabrics for cement composites reinforcement, Asian J. Civ. Eng. (Building and Housing) 12 (5) (2011) 551–562.